Preprint Cambridge Centre for Computational Chemical Engineering ISSN 1473 – 4273

Exploring the internal structure of soot particles using nanoindentation: A reactive molecular dynamics study

Laura Pascazio [1], Jacob W. Martin [1,2], Kimberly Bowal [1], Jethro Akroyd [1,2] and Markus Kraft [1,2,3]

released: 16 October 2019

[1] Department of Chemical Engineering and Biotechnology
University of Cambridge
West Site
Philippa Fawcett Drive
Cambridge, CB3 0AS
United Kingdom
E-mail: mk306@cam.ac.uk

[2] Cambridge Centre for Advanced Research and Education in Singapore (CARES)
CREATE Tower
1 Create Way
Singapore, 138602

[3] School of Chemical and Biomedical Engineering
Nanyang Technological University
62 Nanyang Drive
Singapore, 637459

Preprint No. 241

Keywords: molecular dynamics, reactive force field, hardness, crosslinking, nanoindentation

Edited by
Computational Modelling Group
Department of Chemical Engineering and Biotechnology
University of Cambridge
Philippa Fawcett Drive
Cambridge CB3 0AS
United Kingdom

E-Mail: c4e@cam.ac.uk
World Wide Web: http://como.ceb.cam.ac.uk/

Abstract

The nanoindentation of soot particles is simulated using reactive molecular dynamics to investigate the relationship between the observed mechanical properties and the internal structure of the particles. The particles that are provided as inputs to the simulations are generated using reactive molecular dynamics to create 3D networks of crosslinked coronene, circumanthracene and core-shell mixtures of coronene and circumanthracene. The results of the simulated nanoindentation experiments are analysed as a function of the degree of crosslinking (defined as the number of crosslinks per monomer in the particles), the size and the core-shell structure of the particles. In the case of homogeneous particles (i.e. those without a core-shell structure), the simulations show a unique relationship between the degree of crosslinking (CL) and the simulated hardness, Young's modulus and deformation ratio. In the case of particles with a core-shell structure, a unique relationship was only found by considering the core-shell ratio and the degree of crosslinking in both the core and the shell. Our results coupled with nanoindentation experiments can be used to estimate the degree of crosslinking in soot particles and they show that mature soot must contain crosslinks between its aromatic constituents ($CL > 2$) to be consistent with experimental hardness values.

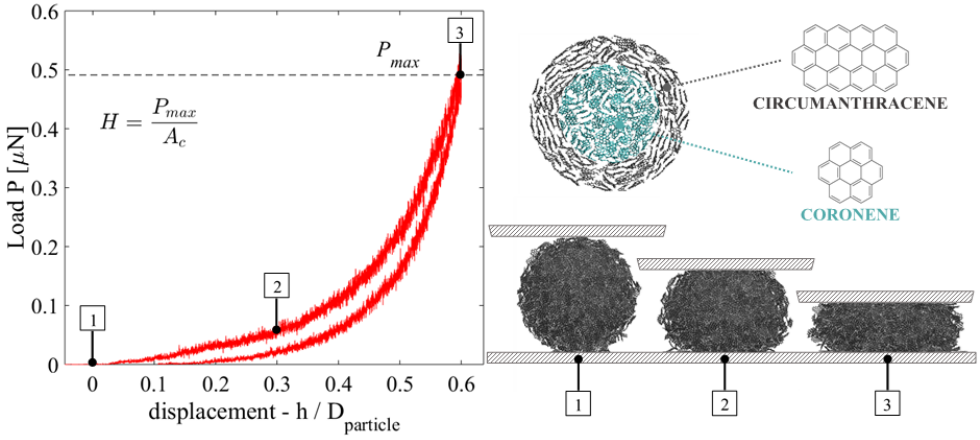

Highlights

- Mechanical properties of crosslinked soot are simulated using reactive MD.
- Soot particles are described as 3D networks of crosslinked PAHs.
- Hardness depends primarily on the degree of crosslinking (CL) and core-shell structure.
- Mature soot must contain $CL > 2$ to be consistent with experimental hardness.

Contents

1 Introduction

Combustion-generated carbonaceous particles, also known as soot, are generally considered to be unwanted byproducts of combustion processes and a significant atmospheric pollutant [5, 28]. Over the last decade, many studies have been conducted on the chemical-physical mechanisms responsible for the formation of carbon compounds in flames [53], with the aim of improving combustion efficiency and reducing the emission of pollutants from combustion devices. Moreover, since such carbon compounds share many common characteristics with industrially-produced carbons (graphene, fullerene, carbon black, etc.), a deeper knowledge of the chemistry and morphology of these carbonaceous particles could be a starting point to develop new flame synthesis routes for functional carbon-based nanomaterials [53].

Transmission electron microscopy has long been applied as a tool to study soot structure [15, 16, 49] and more recently detailed observation and quantification of the internal structure of the particles at the nanoscale can be accessed using high resolution transmission electron microscopy (HR-TEM) and fringe analysis [7, 8, 44, 52, 54]. Young soot particles ($<$10 nm) are characterised by a disordered structure, consisting of short carbon layers with some curvature, which has been interpreted as stacks of polycyclic aromatic hydrocarbon (PAH) molecules [9, 22]. Mature soot primary particles exhibit a core-shell structure consisting of a disordered particle core, potentially with multiple nuclei [22], containing small fringes surrounded by larger stacked fringes [2, 7, 9, 22]. An increase in the C/H ratio and the degree of crystallinity is observed with soot maturity due to a carbonisation process that is responsible for the growth of the graphitic structures and a decrease in the curvature and interlayer spacing [20, 33].

Computational molecular dynamics (MD) and global optimisation methods have also been used to gain insight into the internal structure of soot nanoparticles [36, 40, 47]. Homogeneous clusters containing a single type of PAH molecule are often used as simple analogues of soot particles even though soot particles are known to contain a distribution of PAH molecular sizes [6]. Morphologies of heterogeneous PAH clusters have been recently investigated to understand whether the core-shell structure of soot is due to physical partitioning of different sized PAHs [10]. The simulations found that heterogeneous PAH clusters favour a core-shell structure in which the larger molecules are located closer to the cluster centre. However the inverse morphology was observed experimentally – smaller fringes are found in the core of the particle and larger fringes make up the surface layers – for mature soot particles using HR-TEM [2, 7, 9, 22], indicating that intermolecular interactions are not responsible for the core-shell partitioning seen in mature particles and that crosslinks between PAH molecules might play a crucial role in determining mature soot particle structure. More detailed soot models have also been proposed in literature to represent soot structure. The model proposed by Fernandez-Alos et al. has been created using an automated aromatic structure generation approach directly from HR-TEM lattice fringe images [18]. The models generated by this approach can reproduce the orientation, stacking and distributions of the aromatic moieties within soot but they remain "slice" models that currently do not consider crosslinking and carbonisation.

The presence of crosslinks in soot nanostructures is also important for elucidating information about the very initial stages of soot nanoparticle formation. Reactive aromatic

species that crosslink have long been thought to contribute to soot inception. A variety of chemical pathways in which PAHs react to form crosslinked three-dimensional structures have been proposed [11, 14, 25, 50, 51] and explored in modelling works [21, 30, 31]. Iavarone et al. showed that the presence of covalent bonds among the aromatic subunits improves clustering and growth at high temperature [21]. Mao et al. found that only the PAH dimers formed from PAH radicals through radical-radical combination processes possess a lifetime long enough for subsequent PAH growth [31]. Experimental evidence for the chemical structures of aliphatically substituted and bridged PAH species in gas-phase combustion environments has been reported by Adamson et al. [1]. Nuclear magnetic resonance studies on soot formed by pyrolysis have also shown that soot growth consists not only of PAH molecule growth but also PAH crosslinking [45]. High-resolution atomic force microscopy and photoionisation mass spectrometry have recently confirmed the presence of resonance-stabilised radical (RSR) species [13, 26, 43]. It has been suggested that these RSR species can undergo crosslinking reactions with a variety of hydrocarbons. The product of these crosslinking reactions can be another RSR species, enabling chain reactions to occur [26].

While imaging crosslinks directly in soot particles has been difficult, nanoindentation can provide insight into the structure of the particles. Nanoindentation is an established technique that measures the force as a well-defined tip is pushed into a material, from which the hardness (H) can be determined. The relative hardness of different carbon materials can provide an indicator for the degree of crosslinking. Nanocrystalline graphite is a non-crosslinked structure made of mobile graphene sheets, possessing very low hardness values (0.1-0.4 GPa) [38]. In contrast, soot shows hardness values of 2-8 GPa [3, 4, 23, 24], values closer to a hard crosslinked structure such as charcoal (3-5 GPa) [57]. The wide range found for soot hardness suggests that particles collected at different residence times and produced in different combustion environments may be characterised by different structural properties.

There have been preliminary attempts to incorporate crosslinks into models. Highly graphitised carbon black particles have been constructed from defective concentric fullerene molecules arranged in an onion-like structure with the help of reactive MD [17, 19]. In conjunction with nanoindentation experiments, models have been constructed of nanoparticles with varying degrees of structure but without heteroatoms [24]. These simulations began to explore the impact of a core and shell structure and the hardness of such particles. However, soot particles are known to contain a significant fraction of hydrogen (unlike materials such as carbon black) and are not completely carbonised, so that a new model able to describe soot structure is needed. In a recent paper it was reported that the hardness of crosslinked aromatics increases with the degree of crosslinking in the structure and a range of degree of crosslinking for ethylene and diesel soot particles was estimated [37]. These hardness values were derived from uniaxial tensile test simulations of periodic boxes containing crosslinked PAH through the use of an empirical constant of proportionality. The constant was derived by taking into consideration the fact that soot has an intermediate structure between highly oriented pyrolytic graphite and diamond. These results provided ranges for the degree of crosslinking within soot nanoparticles, but they did not determine the impact of internal nanostructure or allow for a direct comparison with nanoindentation experiments of soot.

The aim of this paper is to simulate the nanoindentation of model soot particles with core-shell structures to provide direct comparison with nanoindentation experiments. The model soot particles that are provided as inputs to the nanoindentation simulations are generated using reactive force field molecular dynamics to create 3D networks of crosslinked PAH arranged in a sphere. To our knowledge, the soot particle model developed here incorporates crosslinks in the soot structure for the first time, where until now the degree of crosslinking has yet to feature prominently in discussions. Structural parameter-mechanical property relationships were derived from nanoindentation simulations of these soot particles. Comparison with nanoindentation experiments performed with *in situ* transmission electron microscopy provided insights into the degree of crosslinking and the internal nanostructure of soot nanoparticles.

2 Methodology

Reactive force field MD simulations were employed to simulate the nanoindentation-induced deformation of model soot particles. All the reactive force field molecular dyanmics simulations were carried out using the LAMMPS software [39]. The interactions within molecules were modelled using an updated version of the adaptive intermolecular reactive empirical bond order (AIREBO) potential [46], known as AIREBO-M [34], which has been widely used to investigate the mechanical and thermal properties of carbon-based nanomaterials [34, 41, 56]. In previous work this method was benchmarked to ensure that it could accurately predict the mechanical properties of PAH molecules [37]. Simulations of tensile tests were used to calculate the Young's modulus for diamond along the <111> and <100> and graphene along the armchair and zig-zag within 4% of the experimental values [29, 42, 56]. Comparisons between crosslinked biphenyl and naphthalene were slightly overestimated by AIREBO-M (+5.5% and +5.0%, respectively) compared with experimental results [48]. The effect of density was seen to have a minimal impact on the yield stress and Young's modulus between 1.5–1.8 g/cm^3.

2.1 Soot particle model construction

The model soot particles used in this work are PAH clusters with a core-shell structure within which medium-sized aromatic components are crosslinked to varying degrees. Figure 1 illustrates the components of the model particle: a quasi-amorphous central core (coloured in blue in Fig. 1) composed of coronene molecules ($C_{24}H_{12}$); an ordered outer shell (coloured in grey in Fig. 1) consisting of circumanthracene molecules ($C_{40}H_{16}$). These starting molecules were selected to match the size of molecules seen experimentally: HR-TEM and fringe analysis results show that the most abundant PAHs in young and mature soot have approximately 7 aromatic rings (coronene) and the fragment size increases with the radial distance from the centre [9]. The larger circumanthracene molecules have therefore been chosen for the particle shell, and coronene molecules for the core. Note that previously, the size of the constituent molecules was shown to have only a weak effect on mechanical properties whereas a primary dependence was found with the degree of crosslinking [37]. We therefore do not expect different starting

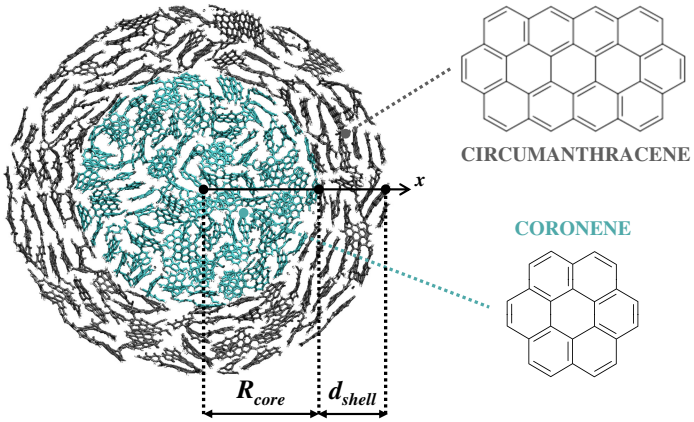

Figure 1: *Structure of a model soot particle consisting of a quasi-amorphous core and an ordered outer shell. Blue and grey colours indicate carbon atoms in the core and shell, respectively. White spheres correspond to hydrogen atoms.*

monomers or a heterogeneous collection of molecules to modify the results significantly.

Spherical particles of crosslinked molecules with diameters from 7–11 nm were prepared for nanoindentation simulations as follows. PACKMOL software [32] was employed to create starting configurations for the crosslinking process. Monomers were randomly located in the quasi-amorphous core and disposed in layers in the "graphitic" shell. The number of molecules was chosen to give a density of 1.5 g/cm^3, which is a typical value for soot particles [55].

The crosslinks between PAH molecules in the particle were created through the same crosslinking procedure that has been developed in a previous publication [37], with core and shell crosslinking reactions run separately. This procedure did not consider a particular crosslinking mechanism as this would require prohibitively long simulations. Instead, reactive sites were generated through the removal of some hydrogen atoms from the rim of the molecule in a manner that allowed single bonds between the aromatics to form. A reactive force field simulation in NVT ensemble was run up to 100 ps and halted at different times to provide varying degrees of crosslinking. A time step of 0.25 fs was adopted for the integration of the atomic equations of motion and the Berendsen thermostat was used to maintain a constant temperature of 1000 K with a time constant of 0.1 ps. These simulation parameters ensured a stable simulation as significant heat had to be removed due to bond formation.

The degree of crosslinking (*CL*) is defined as:

$$CL = \frac{2 \cdot \text{number of crosslinks in the system}}{\text{number of starting monomers}}. \tag{1}$$

CL represents the average number of crosslinks possessed by each molecule in the system. For example, when the *CL* density is 1, each molecule has on average a single crosslink and mainly dimers are formed. A *CL* density of 2 is required for a polymer where on average each molecule has two crosslinks and a *CL* value higher than 2 produces a 3D network of crosslinked PAHs. The degree of crosslinking increases as a function of the simulation time and is reported in Fig. 13 of the Appendix A.1 for all the systems investigated.

Hydrogen atoms were then added back to the sites that did not form crosslinks. Due to the high simulation temperature, a position potential was implemented during the reactive force field MD simulation to reach the desired degree of crosslinking without the loss of molecules from the particle. This added potential acted on molecules located outside of the particle boundary to restrain them within a spherical volume (core) or spherical slice (shell). The simulations were stopped at the desired degree of crosslinking. PACKMOL software [32] was again used to combine the outer shell with the quasi-amorphous core to produce a single model.

More than two hundred different particles were constructed to understand the effect of different structural parameters on the simulated hardness. The parameter ranges for the particles considered in this study are summarised in Table 1.

Table 1: *Structural parameters of the investigated model soot particles: degree of crosslinking in the core (CL_{core}), degree of crosslinking in the shell (CL_{shell}), core radius (R_{core}), shell thickness (d_{shell}) and particle radius (R_p).*

Parameter	Min	Max	Units
CL_{core}	0.00	4.00	–
CL_{shell}	0.00	3.30	–
R_{core}	0.00	4.50	nm
d_{shell}	0.00	4.50	nm
R_p	3.50	5.50	nm

2.2 Nanoindentation simulations

Reactive force field MD was employed to simulate the nanoindentation-induced deformation of model soot particles in order to investigate the effect of the structural parameters of the particles on their mechanical properties. The particles were first relaxed at 300 K for 100 ps in the NVT ensemble by using a chain of three Nosé-Hoover thermostats. No position restraint was used and the particles maintained nearly spherical geometries. The initial velocities of the atoms were assigned in accordance with the Maxwell-Boltzmann distribution. Once equilibrated, the nanoparticles were subject to indentation. The setup for the nanoindentation simulations is shown in Fig. 2. The time step was set as 0.5 fs. A virtual wall was placed at the bottom of the particle. The indentation simulations were performed with a planar indenter initially placed 5 Å above the particle. The choice of a planar indenter instead of a spherical one (used in experimental studies) comes from the small size of nanoparticles compared to the typical size of indenter tips. Then, the planar approximation can be used. The simulation was made up of three stages: a loading stage in which the indenter moved downwards at a constant speed of 25 m/s (a study of the appropriateness of the indentation speed can be found in the Appendix A.3) up to a maximum indentation depth of 0.6 times the initial particle diameter, which is the maximum indentation depth used in soot nanoindentation experiments [23, 24]; a constant load stage in which the indenter was at the maximum indentation depth for 50 ps; and an unloading stage in which the indenter moved upwards up to its starting position at the same speed used during the loading stage. The displacement function is reported in Fig. 3b.

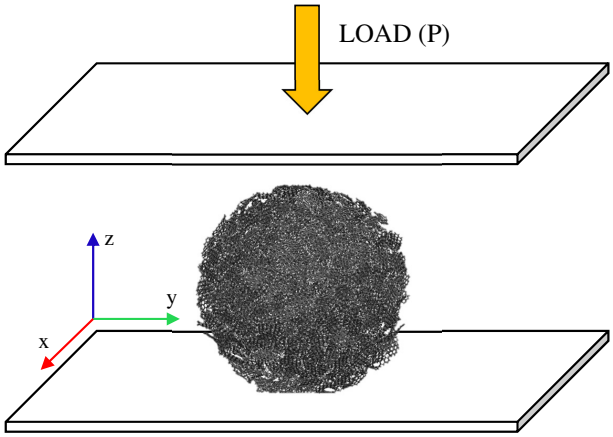

Figure 2: *Molecular dynamics model of a particle of crosslinked coronene molecules for nanoindentation with a planar indenter.*

2.3 Estimation of mechanical properties

The mechanical properties of a given material can be derived from the loading/unloading curve [35]. The hardness (H) of the particle can be calculated as follows:

$$H = \frac{P_{\max}}{A_c} \tag{2}$$

where $P_{\max}$ is the maximum force acting on the indenter at the end of the loading stage and A_c is the contact area calculated from the atomic positions at the maximum load [35]. The contact area was calculated as the spherical approximation of the convex hull of the atoms in contact with the surface of the indenter. This spherical approximation mirrors the experimental procedure [23], which is unable to record the real contact area and instead considers a circle derived from the 2D image recorded during nanoindentation. Additional details about the contact area calculations are reported in the Appendix (A.2). The nanoindentation curve features thermal fluctuation; for this reason 50 ps of simulation time were added at the maximum load, shown as $(t_2 - t_1)$ in Fig. 3b. The mean values of P and A_c obtained over this time were used in the calculation ($P_{\max} = \overline{P}(h_{\max})$, $A_c = \overline{A_c}(h_{\max})$). The elastic modulus ($E$) of the particle can be obtained from the relationship:

$$\frac{1}{E_r} = \frac{(1-\nu^2)}{E} + \frac{(1-\nu_i{}^2)}{E_i} \tag{3}$$

where ν and ν_i are the Poisson's ratios of the particle and the indenter, respectively. E_i is the elastic modulus of the indenter and E_r is the reduced modulus, which takes into account the induced elastic deformations in both the indenter and the particle [35]. For our work, where the indenter was modelled as a fully rigid body, the value of E_i is infinite; thus, the equation simplifies to:

$$E = E_r(1-\nu^2). \tag{4}$$

The Poisson's ratio of the particle was calculated as described in Appendix A.4. The value of E_r is given as:

$$E_r = \frac{\sqrt{\pi}}{2} \cdot \frac{S_{max}}{\sqrt{A}} \tag{5}$$

where S_{max} is the slope of the unloading curve at the maximum load and A is the contact area at the maximum load [35]. Some of these quantities are shown in Fig. 3a.

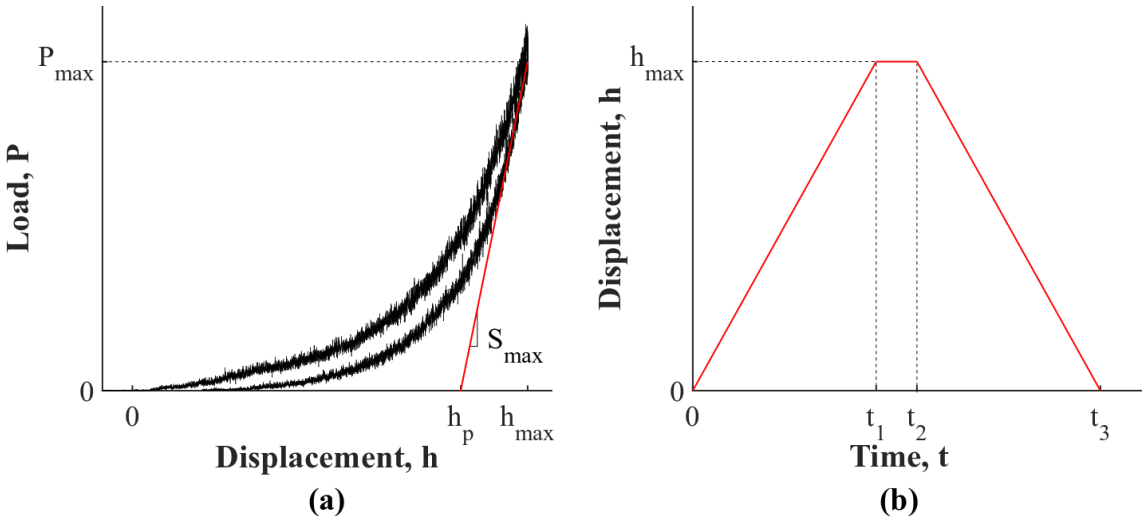

Figure 3: *(a) Illustration of the load-displacement curve and the parameters used in the calculations of hardness and Young's modulus. (b) The displacement-time function used during the indentation simulations.*

3 Results

3.1 Particles without shell

The effects of crosslinking and particle diameter on particle mechanical properties are first examined for model soot particles without a surrounding shell (i.e. consisting of a core only). Figure 4 shows the load-displacement $(P-h)$ curves of nanoindentation for these model particles without shells. The particles have a 7 nm diameter and varying degrees of crosslinking. The particles exhibit elasto-plastic behaviour as in previous nanoindentation experiments [3, 4, 24]. It can be observed that the maximum load and the slope of the curves increases with the degree of crosslinking in the particle. The maximum load increases from 0.003 μN (noncrosslinked PAH) to 0.33 μN (CL=3.5). This is expected since the higher the degree of crosslinking, the stiffer the particle.

From these type of curve it is possible to compute the hardness and Young's modulus using Eq. 2 and 4. These quantities are reported in Fig. 5 for particles of different sizes and with varying degrees of crosslinking. The obtained values all arrange around the same line, indicating that they are not affected by the particle size. The hardness and

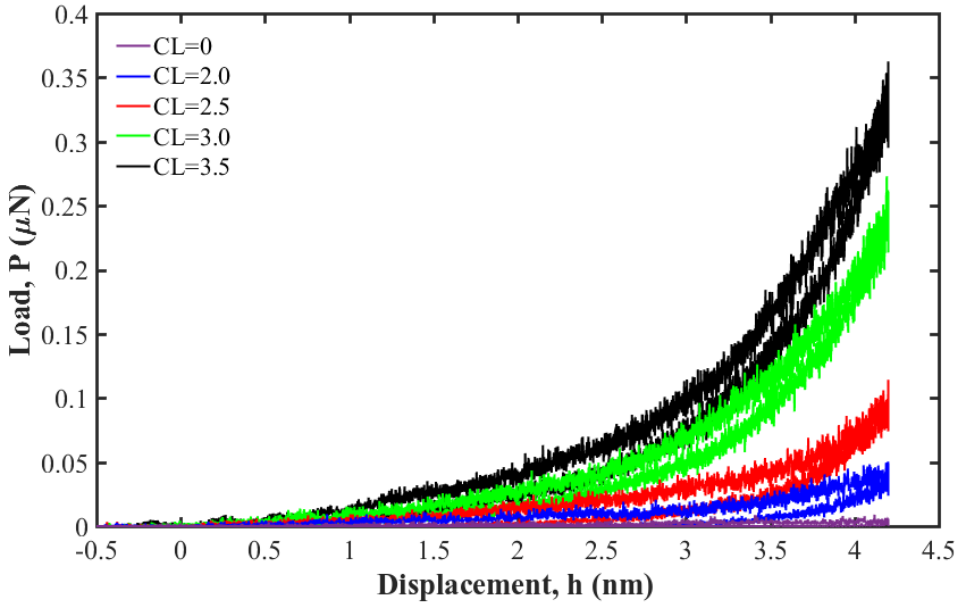

Figure 4: *The load-displacement curves of particles with 7 nm diameter, without shells and with varying degrees of crosslinking (CL).*

the Young's modulus increase with the degree of crosslinking, which is consistent with what was obtained from uniaxial tensile test simulations [37]. From a microscopic perspective, this behaviour can be explained as follows: the crosslinking between monomers strengthens the material so that when $CL < 2$ (values corresponding to PAH oligomers) the material shows a hardness value lower than 1 GPa. It increases almost linearly when $CL > 2$ (value corresponding to a 3D crosslinked structure of PAH), up to a value of around 8 GPa when $CL \approx 3.5$. Similar considerations can be made for the Young's modulus (E). The Young's modulus increases with increasing CL, which means that the elastic recovery is larger at a higher CL. The linear dependence of the hardness and the Young's modulus for $CL > 2.5$ indicates that every crosslink present in the structure contributes to its mechanical properties, resulting in a direct proportionality relationship.

The Young's modulus is an indicator of a particle's elastic response. However, it cannot be used as an indicator of a particle's plastic behaviour. The hysteresis in the loading/unloading curve indicates that plastic deformation is occurring in the particle. An indicator of the plasticity of the particle is the deformation ratio defined as the ratio between the final and initial height of the particle (z_f/z_i). Figure 6 shows particles with varying degrees of crosslinking before the loading stage (Fig. 6b), at the maximum load (Fig. 6c) and after the unloading stage (Fig. 6d). When $CL = 0$ the final height (height after the unloading stage) of the particle is very similar to the height of the particle at the maximum load, indicating a fully plastic behavior. The final/initial height ratio is around 0.4 times the particle diameter, corresponding exactly to the difference between the initial height and the maximum indentation depth (0.6 times the particle diameter) as reported in Fig. 6a. When $CL \approx 3.5$, $z_f/z_i \approx 0.9$, indicating that the final height of the particle is almost equal to its initial height. CL values in between these two extremes show an intermediate behaviour, with elasticity increasing with CL.

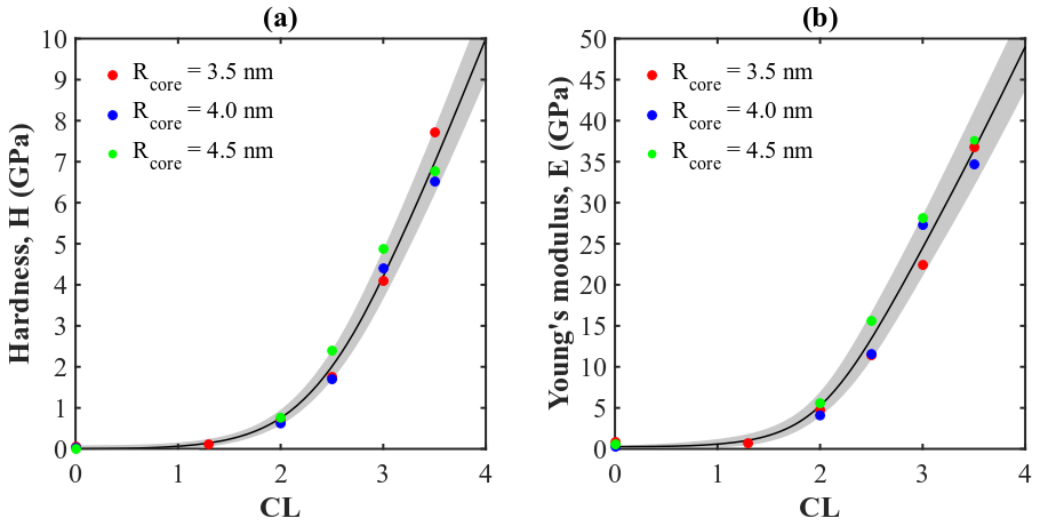

Figure 5: *(a) Hardness (H) and (b) Young's modulus (E) as a function of the degree of crosslinking in the particle (CL). Different colours correspond to different particle sizes. The black lines and grey areas are provided to show the value ranges across the different simulations.*

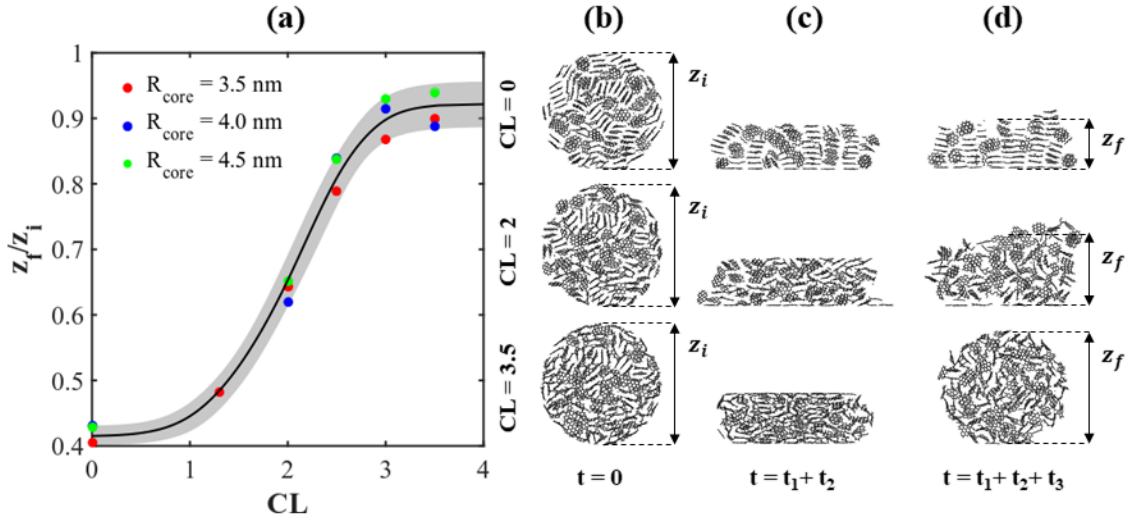

Figure 6: *a) The deformation ratio (z_f/z_i) as a function of the degree of crosslinking in the particle (CL). Different colours correspond to different particle sizes. The black line and grey shading are guides to visualise the trend and range of values obtained for the z_f/z_i values. b) Screenshots of particles with varying degrees of crosslinking before the loading stage, c) at the maximum load and d) and after the unloading stage.*

The behaviour of a particle under compression can be compared with the collision of a particle with a surface. AFM experiments on soot particles collected by thermophoretic sampling on a mica disc in a premixed ethylene flame showed that particles with a diameter less than 5 nm are very flat, while the thickness and sphericity increased with the size

of the particle, indicating a more rigid structure [12]. These smaller plastic deformations might result from crosslinking reactions involved in particle growth and therefore in an increased *CL*.

In summary, for a particle without a shell, the mechanical properties are a function of the degree of crosslinking in the structure with hardness and elasticity increasing with an increase in *CL*. These properties do not depend on the particle diameter.

3.2 Core-shell particles

In this section, we investigate the effect of adding an ordered shell around the PAH crosslinked core. Figure 7 compares the load-displacement curves of particles with a diameter of 9 nm, shell thickness of 1 nm, $CL_{\text{core}} = 2.5$ and varying CL_{shell} with the response of a shell-free particle with the same size and same CL_{core} (black line in Fig. 7). This allows us to explore the effect of different values of CL_{shell}. When $CL_{\text{shell}} < CL_{\text{core}}$, the load shows a delay (defined as the difference in displacement for a specified load) compared to the reference particle with no shell. The core-shell particle provides the same load after a delay that is almost equal to twice the shell thickness when $CL_{\text{shell}} = 0$. This delay decreases with CL_{shell} until $CL_{\text{shell}} = CL_{\text{core}}$ where the two load curves almost overlap. This is expected because the total degree of crosslinking is lower than or equal to the total degree of crosslinking in the reference particle. When $CL_{\text{shell}} > CL_{\text{core}}$, core-shell particle load curve provides the same load at a lower indentation depth.

In Fig. 8 the hardness of core-shell particles is compared across different sizes and nor-

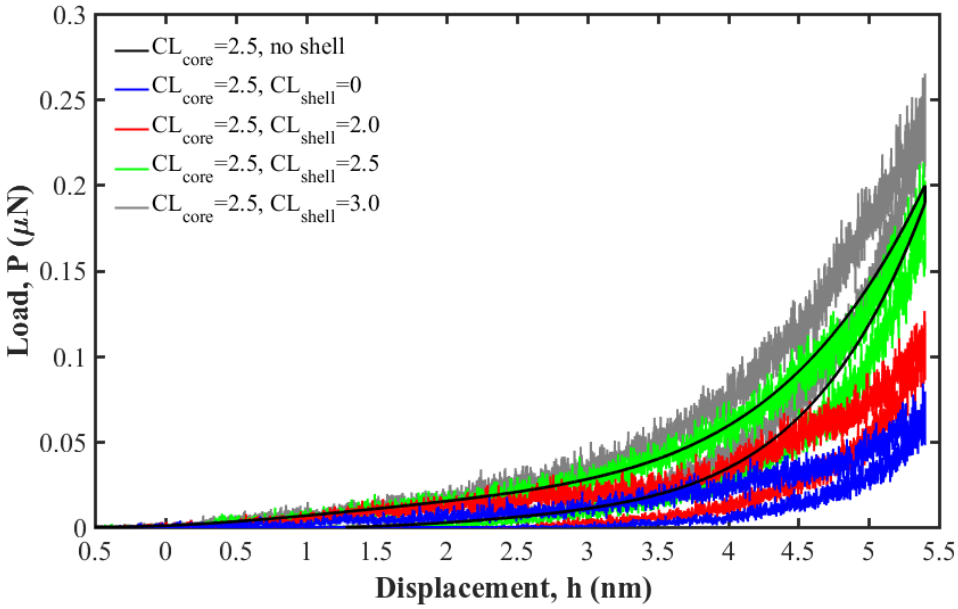

Figure 7: *The load-displacement curves of particles with a 9 nm diameter,* $CL_{\text{core}} = 2.5$, $d_{\text{shell}} = 1$ *nm and with varying degrees of crosslinking in the shell (*CL_{shell}*). The black line refers to a shell-free particle with the same size (9 nm) and* $CL_{\text{core}} = 2.5$.

malized shell thickness as a function of the total degree of crosslinking. The normalized shell thickness is define as the shell thickness-particle radius ratio ($d_{\text{shell}}/R_{\text{p}}$). Particles without shell are composed of coronene molecules disposed in a disordered way and they have a value of the normalized shell thickness of zero. Oppositely, a particle composed entirely of circumanthracene molecules disposed in layers has a normalized shell thickness value of 1. Core-shell particle have a normalized shell thickness that goes from 0 to 1 decreasing the core-shell ratio. The total degree of crosslinking is calculated as follows:

$$CL_{\text{tot}} = \frac{n_{molecules,core} \cdot CL_{\text{core}} + n_{molecules,shell} \cdot CL_{\text{shell}}}{n_{molecules,core} + n_{molecules,shell}}. \tag{6}$$

As opposed to the behaviour shown for particles without shells, the hardness values are not simply a function of the total CL in the particle (black line in Fig. 8) and show a large degree of scatter. In particular, at a given value of normalized shell thickness (shown in different colours in Fig. 8), different combinations of degrees of crosslinking in the shell and in the core can give the same hardness value. This suggests that the hardness value is influenced by the distribution of crosslinks in the core and the shell.

In Fig. 9, hardness values for particles with a fixed value for the degree of crosslinking in the core ($CL_{\text{core}} = 2.5$) are reported as a function of the normalized shell thickness ($d_{\text{shell}}/R_{\text{p}}$) and at different CL_{shell} values. The first thing to note is that when the degree of crosslinking is homogeneously distributed in the particle ($CL_{\text{shell}} = CL_{\text{core}}$) the hardness value is not affected by the monomer size or monomer arrangement since similar hardness values are found within the entire normalized shell thickness range (horizontal line in

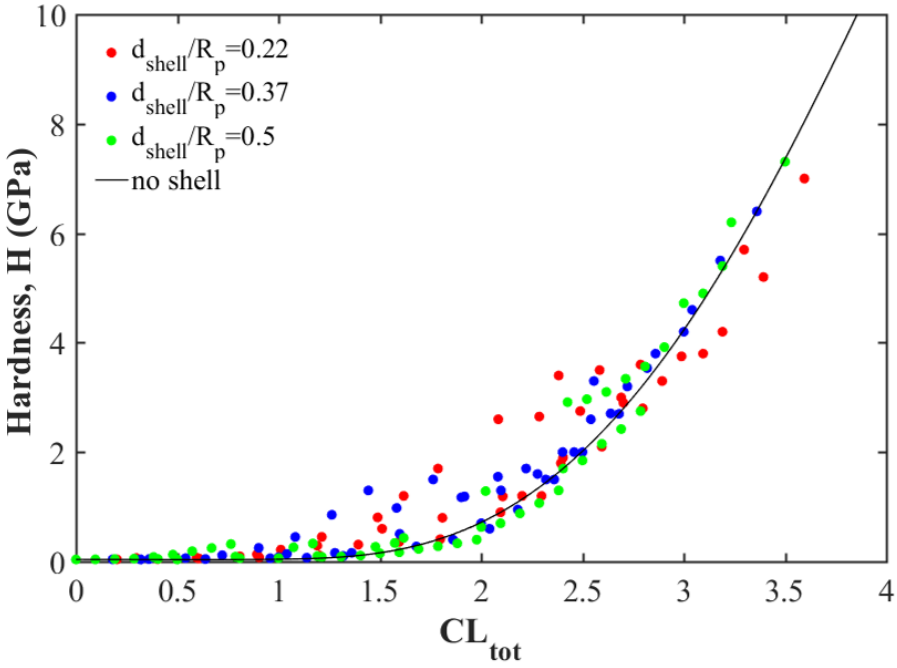

Figure 8: *Hardness (H) as a function of the total degree of crosslinking in the particle (CL_{tot}). Different colours correspond to different normalized shell thickness. The black line refers to particles without shells.*

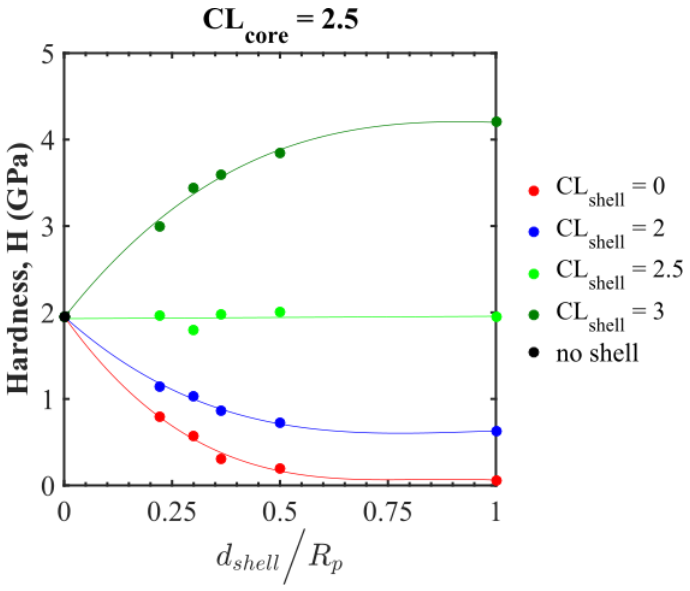

Figure 9: *Hardness (H) as a function of the normalized shell thickness ($d_{\text{shell}}/R_{\text{p}}$) for particles with $CL_{\text{core}} = 2.5$. Different colours correspond to particles with different CL_{shell} values.*

Fig. 9). This means that the results shown in Fig. 5 are always valid when the particle has a homogeneous degree of crosslinking. Conversely, when the degree of crosslinking is not homogeneous ($CL_{\text{shell}} \neq CL_{\text{core}}$), the particle hardness value is comparatively higher or lower. Another observation from Fig. 9 is that when the shell becomes big enough ($d_{\text{shell}}/R_{\text{p}} > 0.7$) the hardness curve reaches a plateau and the shell completely shields the effect of the core, giving the same results as the homogeneous case where CL is equal to CL_{shell}. Therefore, the mechanical properties are mainly dependent on the particle surface properties. In fact, a very thin shell can produce considerable variations in the mechanical properties and a very thick shell can completely shield the contribution of the structural properties of the core on the mechanical properties of the particle.

Finally, all the data obtained for more than 200 particles with different structural parameters (particle diameter, core/shell ratio, CL_{core} and CL_{shell}) have been fitted to contoured 3D surface plots and reported in Fig. 10. These plots show the dependence of hardness, Young's modulus and deformation ratio ($z_{\text{f}}/z_{\text{i}}$) on the degree of crosslinking in the core and the shell for particles with three different values of normalized shell thickness (0.22, 0.37 and 0.5). As it is possible to note, when the normalized shell thickness is low (left-hand column) the properties are strongly dependent on both the CL_{core} and CL_{shell}, and as the shell thickness increases, the shell contribution becomes more important. In fact, when the normalized shell thickness is 0.5 it is already clear that the mechanical properties are mainly dictated by the degree of crosslinking in the shell. These contour plots can be used to estimate the degree of crosslinking in the particle from experimental studies of the mechanical and structural properties of soot particles, as discussed in the next section.

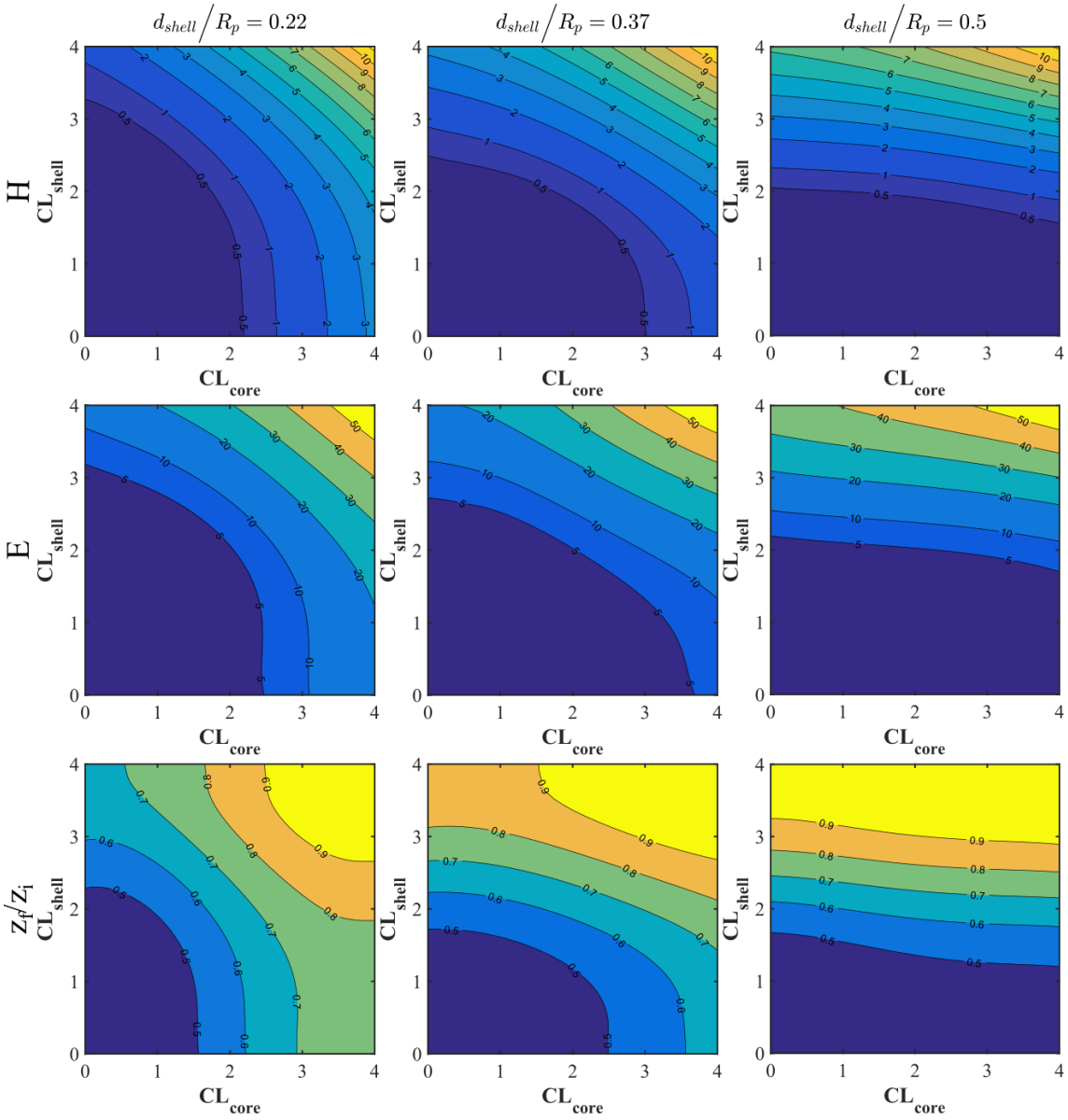

Figure 10: *Hardness (H) (first row), Young's modulus (E) (second row) and deformation ratio (z_f/z_i) (third row) as a function of the degree of crosslinking in the core (CL_{core}) and the shell (CL_{shell}) at three different normalized shell thickness (d_{shell}/R_p): 0.22 (first column), 0.37 (second column) and 0.5 (third column).*

4 Discussion

We now summarise the simulation results for the purpose of interpreting experimental nanoindentation studies as follows.

For a particle in which the shell is not yet formed (representative of a young soot particle [9]):

1. Particles with low *CL* values have a very low hardness. The hardness increases as a

function of the CL in the structure. This is linear with CL when CL is higher than 2.

2. The mechanical properties (hardness, Young's modulus) do not depend on the particle diameter.

3. The mechanical properties do not depend on the size of the starting monomer or monomer arrangement, indicating that the shell-free particle results can be used also for particles where the degree of crosslinking is homogeneously distributed throughout the particle, irrespective of the distribution of monomers within the particle.

For a core-shell particle (representative of a mature soot particle [9]):

1. The mechanical properties depend on CL_{core}, CL_{shell} and the core/shell ratio.

2. When the shell becomes large enough ($d_{\text{shell}}/R_{\text{p}} > 0.7$), it shields the effect of the core.

These results provide guidelines to aid in relating the mechanical properties and the internal nanostructure of soot particles.

With the knowledge of these relationships, it is possible to estimate ranges for the degree of crosslinking in the core and shell of a soot particle, given its shell thickness and mechanical properties. The figure shows results for a diesel soot particle tested by nanoindentation (particle D1B in Ref. [23]), with the relevant experimental details and crosslinking results shown in Fig. 11. The particle has a hardness value of 2.5 GPa and Young's modulus of 21 GPa (see Appendix A.5 for full details of the analysis). HR-TEM images of this particle also allow the evaluation of the normalized shell thickness ($d_{\text{shell}}/R_{\text{p}} \approx 0.4$) and deformation ratio ($z_{\text{f}}/z_{\text{i}} = 0.84$). The contour plot with the closest $d_{\text{shell}}/R_{\text{p}}$ ratio ($d_{\text{shell}}/R_{\text{p}} = 0.37$) has been selected from Fig. 10. From this contour plot, it was possible to extract hardness, Young's modulus and deformation ratio contour lines with values of particle D1B in the CL_{core}-CL_{shell} plane. The ranges of CL_{core} and CL_{shell} that give those values of mechanical properties across the different simulations of particles with same $d_{\text{shell}}/R_{\text{p}}$ are also reported (shaded areas). The region where the contours intersect shows the range of possible values for the degrees of crosslinking of the core and shell for the soot D1B particle ($CL_{\text{core}} = 1.5-3$ and $CL_{\text{shell}} = 2.6-3.4$). A simulated TEM image of a particle with degree of crosslinking in the core and shell in the range found for particle D1B has also been reported in Fig. 11 (see Appendix A.5 for further details on the method adopted for the TEM image simulation). Unfortunately, we were only able to determine detailed crosslinking information for one particle. All other experiments reported were not made on primary particles but on small aggregates (such as D1A or D2C in [23]) and/or the load displacement curve were not reported.

Another nanoindentation study provides experimental results that are used to estimate the degree of crosslinking for soot particles at different stages in the flame [3]. In Fig. 12, experimental values of the hardness, particle diameter, shell thickness and core diameter for ethylene soot particles at different heights above the burner (HAB) are shown in red. Soot particle size increased with the height above the burner up to HAB = 5.0 cm, followed by a reduction in size due to oxidation at a longer distance from the flame base. The

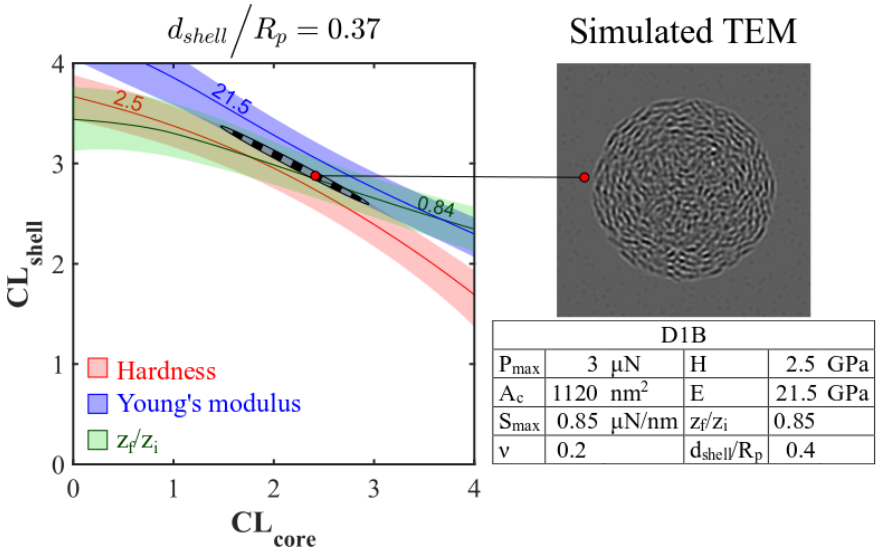

D1B			
P_{max}	3 μN	H	2.5 GPa
A_c	1120 nm^2	E	21.5 GPa
S_{max}	0.85 μN/nm	z_f/z_i	0.85
ν	0.2	d_{shell}/R_p	0.4

Figure 11: *Hardness (H) (red), Young's modulus (E) (blue) and deformation ratio (z_f/z_i) (green) contour lines with error bounds (shaded areas) in the $CL_{core} - CL_{shell}$ plane for the particle D1B tested with nanoindentation in Ref. [23]. The striped area indicates the range of possible values of CL_{core} and CL_{shell} for the particle D1B. A table that summarizes the mechanical and structural properties of particle D1B and a simulated TEM image of a particle with degree of crosslinking in the core and shell in the range found for particle D1B has also been reported.*

particles taken at HAB = 0.5 cm were disordered and have no shell. Above HAB = 0.5 cm, the diameters of the particle cores were reduced and the shell thicknesses increased with increasing HAB until 5 cm. When HAB = 7.0 cm a distinct central (spherical) core is no longer visible. The hardness was 3.5 GPa for the particle at HAB = 0.5 cm and it decreased slightly (H = 3.0 GPa at HAB = 2.0 cm) when the shell started to form, only to increase again up to a value of 4.5 at HAB = 7.0 cm. Using the results for a particle composed of only a core (Fig. 5) and assuming that they are not dependent on the monomer size or arrangement (as suggested from our results in Fig. 9), the degree of crosslinking of the particles collected at 0.5 cm and 7.0 cm were estimated from their experimental hardness values and found to be 2.8 and 3.1, respectively. In the case of a core-shell particle, the degree of crosslinking in the core and shell are two free parameters that cannot be both estimated from the particle hardness alone. One parameter must be assumed to estimate the other. Two possible behavioural assumptions can be assigned to particles with a shell. The first is that the degree of crosslinking does not increase when the shell starts to form (case 1 in Fig. 12) and the second is that the degree of crosslinking in the core increases with the heights above the burner (case 2 in Fig. 12). It is unlikely that the degree of crosslinking in the core decreases with the heights above the burner, knowing that the particles at the top of the flame are found to have a higher degree of crosslinking compared to those at the bottom. Starting from these assumptions, it is possible to estimate the degree of crosslinking in the shell at the required normalized shell thickness using a linear fitting between those obtained from the contour plots in Fig. 10 at

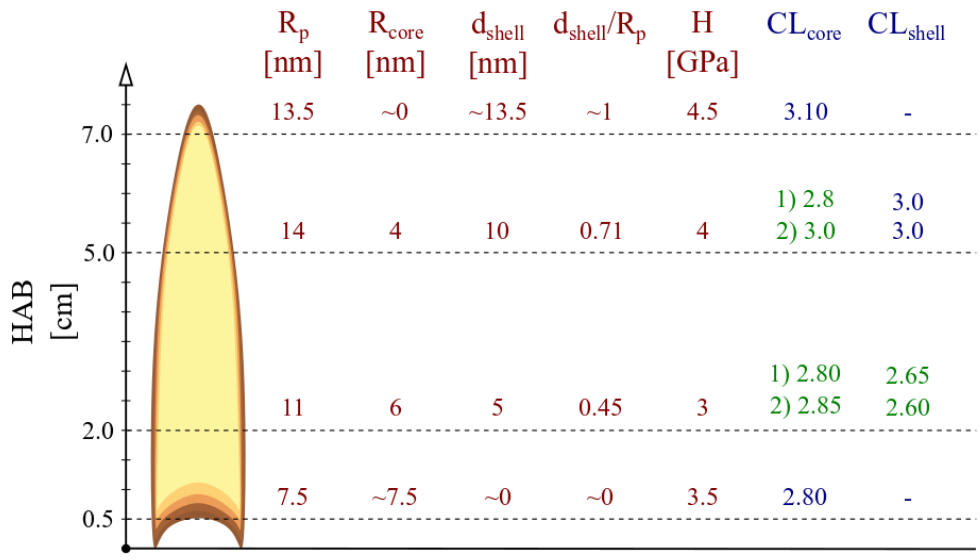

Figure 12: *Experimental values (red) taken from Ref. [3] of the average particle radius (R_p), core radius (R_{core}), shell thickness (d_{shell}), normalized shell thickness (d_{shell}/R_p) and hardness (H) of ethylene soot particles collected at different heights above the burner (HAB) and the estimated (blue) and assumed (green) degrees of crosslinking in the core (CL_{core}) and in the shell (CL_{shell}).*

different normalized shell thickness. The values are marked in green in Fig. 12 if subject to assumptions and in blue if not subject to assumptions. The degrees of crosslinking in the core and in the shell are around 2.8 and 2.6 respectively for the particles collected at HAB = 2.0 cm. At HAB = 5.0 cm, the normalized shell thickness is higher than 0.7 such that the contribution of the core to the overall hardness is negligible and the degree of crosslinking in the shell can be again obtained from the homogeneous case.

Another assumption made in our model is that the particle is composed of only two regions that present different properties. Mechanical properties are strongly dependent on the distribution of crosslinks inside the particle and more layers with different degrees of crosslinking may be present in soot structures. The inclusion of regions with different CL may lead to modified results. However, although our results are subject to a variety of assumptions, we consider that these assumptions are reasonable for a preliminary exploration of the internal structure inaccessible to HR-TEM. Additional techniques would greatly improve the methodologies presented here, such as solid state NMR or atomic force microscopy studies. One general result is that while the simulated hardness values for crosslinked PAH clusters can range from very near to zero to 11 GPa for $CL = 0-4$, from experimental soot hardness the degree of crosslinking of mature soot particles are all found to lie between 2.6 and 3.1, indicating a significant number of crosslinks and the importance of considering crosslinks when developing accurate soot models.

A phenomenological model of soot formation can also be suggested from these results. Soot nuclei (1–3 nm) are thought to be formed by the collision of PAH, either in the form of individual molecules or radicals or clusters of molecules or radicals. The incipient particle contain species that may interact chemically (i.e. PAHs connected by aliphatic bonds) and physically (i.e. formation of stacks of polyaromatic units) and have a degree

of crosslinking between 0 and 2. As shown in Section 3.1, these particles are characterised by low hardness values and deform plastically. This is consistent with the liquid-like behaviour that incipient soot particles show at high temperatures. Further increases in particle size are presumed to occur by the condensation of PAHs from the gas-phase and the formation of a 3D network of crosslinked PAHs, with the degree of crosslinking increasing as they move up the flame. The development of a core-shell structure comes from two different processes: 1) the decrease in the core diameter suggests that some of the aliphatic components surronding the/in the core graphitise after the formation of the initial shell, with the same effect also being responsible for the fringe length increase observed in HR-TEM experiments; 2) the increase in particle size and the lower degree of crosslinking found in the shell with respect to the core and its increase traversing the flame suggests that PAHs of bigger sizes are still condensing from the gas-phase. At the later stages, oxidation is responsible for the particle size decrease.

Unfortunately only few nanoindentation experiments were performed on soot particles. We hope that our results can motivate more experimental nanoindentation work in order to elucidate a clearer description of what occurs during soot formation, especially with regards to young soot particles and particles with a thin shell around their core. These will shed light on the mechanism involved in the first stages of core and shell formation.

5 Conclusions

The nanoindentation of soot particles is simulated using reactive force field molecular dynamics to investigate their mechanical properties as a function of the degree of crosslinking (defined as the number of crosslinks per monomer in the particles) and the size and core-shell structure of the particles. The particles that are provided as inputs to the simulations are generated using reactive force field molecular dynamics to create 3D networks of crosslinked coronene, circumanthracene and core-shell mixtures of coronene and circumanthracene.

In the case of homogeneous particles (i.e. those without a core-shell structure), the simulations show a unique relationship between the degree of crosslinking and the simulated hardness, Young's modulus and deformation ratio. The relationship is independent of particle size, monomer size and monomer arrangement. In the case of particles with a core-shell structure, a unique relationship was only found by considering the core-shell ratio and the degree of crosslinking in both the core and the shell. It was observed that the mechanical properties are mainly dependent on the particle surface properties. In fact, even a very thin shell was able to cause a large change in the properties of the particles and a very thick shell was able to completely shield the contribution of the structural properties of the core on the mechanical properties of the particle.

Our results coupled with nanoindentation and HR-TEM experiments can be used to estimate the degree of crosslinking in soot particles. The complex structure of soot and the difficulties in performing nanoindentation work make the estimation of the degree of crosslinking nontrivial and subject to assumptions. However, we have provided some preliminary results suggesting ranges of crosslink densities, how they evolve as soot particles mature in a flame and how the structural parameters can influence the mechanical

properties of soot particles. To our knowledge, the soot model developed here is the most detailed to date, where until now the degree of crosslinking has yet to feature prominently in discussions. Further analysis requires comparison with other experimental techniques to probe soot properties.

Acknowledgements

This project is supported by the National Research Foundation (NRF), Prime Minister's Office, Singapore under its Campus for Research Excellence and Technological Enterprise (CREATE) programme. This project has received funding from the European Union's Horizon 2020 Research and Innovation Programme under grant agreement no. 724145. This work used the ARCHER UK National Supercomputing Service (http://www.archer.ac.uk).

Nomenclature

A_c	Contact area
CL_{core}	Degree of crosslinking in the core
CL_{shell}	Degree of crosslinking in the shell
CL_{tot}	Total degree of crosslinking
d_{shell}	Shell thickness
d_{shell}/R_p	Normalized shell thickness
E	Young's modulus or elastic modulus
E_i	Elastic modulus of the indenter
E_r	Reduced modulus
H	Hardness
HAB	Height above the burner
h	Displacement
h_{max}	Maximum indentation depth
ν	Poisson's ratio
ν_i	Poisson's ratio of the indenter
P	Load
P_{max}	Maximum load
R_{core}	Core radius
R_p	Particle radius
S	Slope of the unloading curve
S_{max}	Slope of the unloading curve at the maximum load
t_1	Time at the end of the loading stage
t_2	Time at the end of the constant load stage
t_3	Time at the end of the unloading stage
z_i	Initial height of the particle (particle diameter)
z_f	Final height of the particle
z_f/z_i	Deformation ratio

A Appendix

A.1 Crosslinking procedure

Following the procedure implemented in Ref. [37], particles with varying degree of crosslinking (*CL*) were obtained by halting the reactive MD simulations at different simulation times. The reactive sites were created at the start of each simulation in every particle by directly removing 3 or 6 hydrogen atoms in the coronene case, and 4 or 6 hydrogen atoms in the circumanthracene case from the rim of every starting molecule, thus providing systems with low or high *CL* respectively. The *CL* vs time is reported in Fig. 13 for all the systems and cases. The notation core-*x* and shell-*x*-*y* will be used to describe the core and shell cases respectively, where *x* refers to the core radius and *y* refers to the particle radius in Å. Other information such as the number of atoms and H/C ratio related to the models are reported in Table 2.

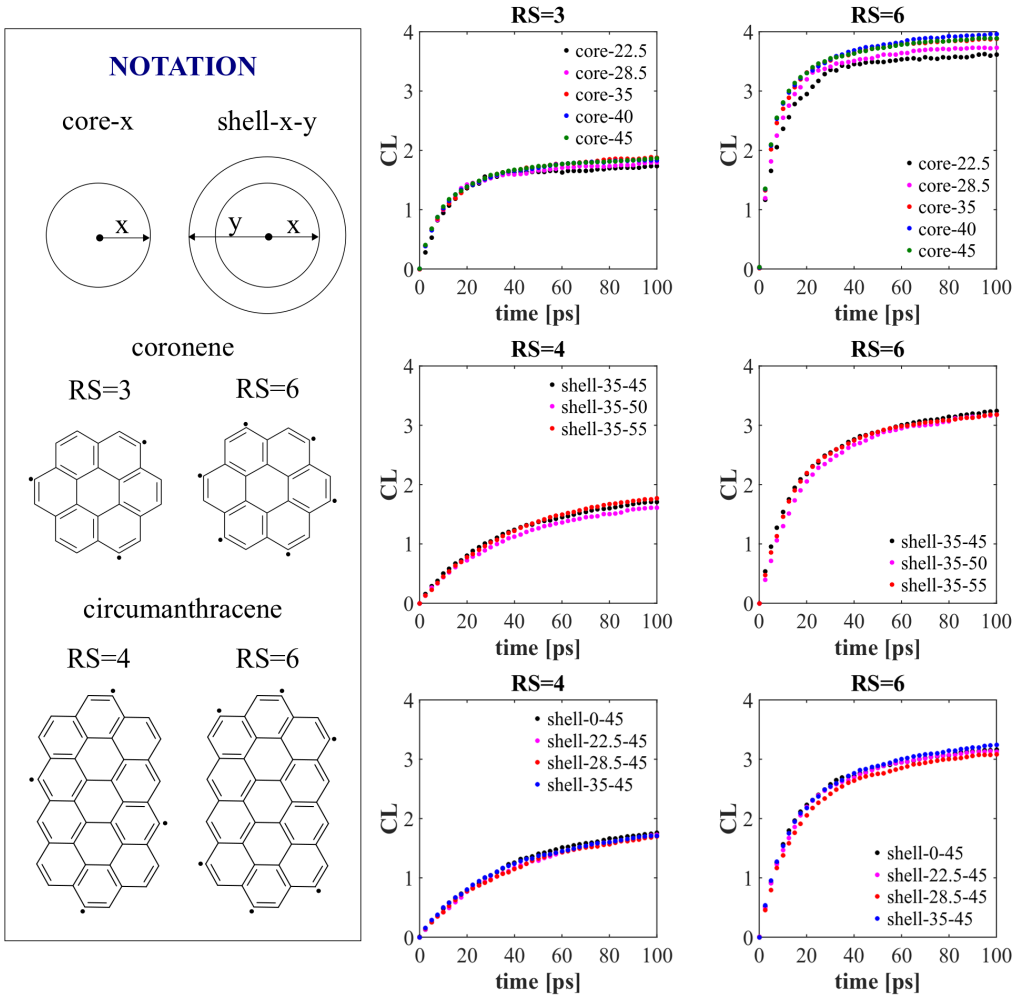

Figure 13: *Degree of crosslinking (CL) as a function of MD time for all the investigated systems.*

Table 2: *H/C ratio and number of atoms ranges of the investigated model soot particles.*

Parameter	min	max
H/C	0.3	0.5
n_{atoms}	20000	72000

A.2 Contact area calculation

The contact area at the maximum load (A_c) was calculated as follow:

1. The contacting atoms of the particle with the indenter were selected every 10 ps during the constant load stage from their coordinates. An atom was considered to be a contacting atom if its z coordinate was equal to the z coordinate of the indenter at the constant load stage ($z = h_{max} = 0.6 \cdot D_p$ being the the z-axis the loading direction and the origin placed at indentation depth equal to zero).

2. The convex hull of every set of contacting atoms was constructed. The distances between the atoms belonging to the convex hulls and the center of mass of the contacting atoms (r_i in Fig. 14) were calculated.

3. The contact area of every convex hull was calculated as the area of the circle with radius equal to the mean values of the distances r_i ($\bar{r}$ in Fig. 14).

4. The constant load stage lasted 50 ps meaning that 5 different areas were calculated for each case. The contact area (A_c) was then calculated as the mean value of the 5 areas.

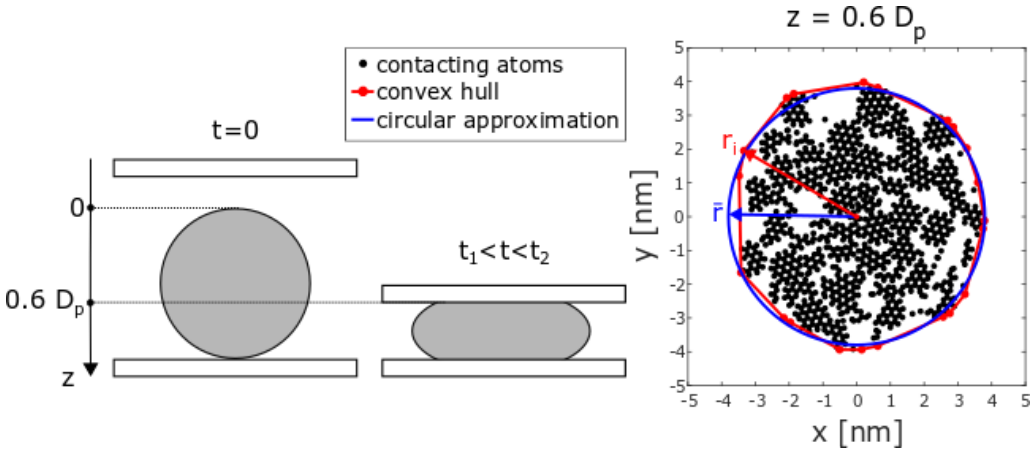

Figure 14: *Contact area at the maximum load: contacting atoms with the indenter (black), convex hull of the contacting atom (red) and its circular approximation (blue).*

A.3 Effect of the indentation speed

In order to investigate the effect of the indentation speed on the mechanical properties, three different indentation speed, i.e., 50 m/s, 25 m/s and 12.5 m/s were considered. Figure 15 shows the load–displacement curves at different strain rates for the 7 nm diameter particle with $CL = 3$. The load displacement behaviour was shown to be insensitive to the choice of indentation speed within this range. An indentation speed of 25 m/s was used for all of the simulations.

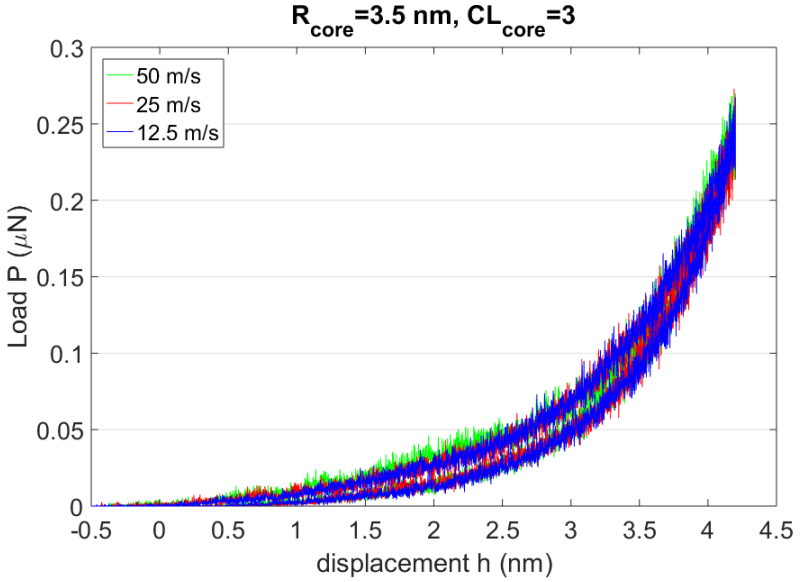

Figure 15: *Load-displacement curves at different indentation speeds for a coronene particle of 7 nm diameter and CL = 3.*

A.4 Poisson's ratio calculation

Boxes of crosslinked coronene molecules with the box having side length 43 Å and a density of 1.5 g/cm^3, have been built as described in a previous publication [37]. The Poisson's ratio ν can be obtained from uniaxial tensile molecular dynamics simulations. The simulation setup is described in Ref. [37].

The Poisson's ratio is defined as:

$$\nu = -\frac{\varepsilon_{\text{lat}}}{\varepsilon} = -\frac{\Delta L'}{\Delta L}. \tag{A.1}$$

where ε is the strain in the tensile direction and ε_{lat} is the lateral strain ($\varepsilon_{\text{lat}} < 0$) measured along one of the directions orthogonal to the vector of the imposed strain.

In Fig. 16, the Poisson's ratio is reported as a function of the degree of crosslinking in the structure.

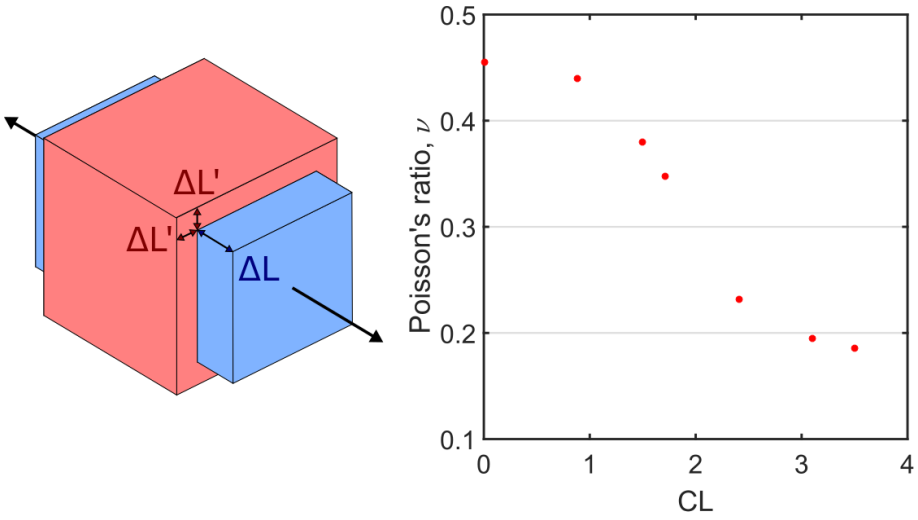

Figure 16: *(b) Poisson's ratio (ν) of periodic boxes of crosslinked coronene molecules as a function of the degree of crosslinking (CL).*

A.5 Analysis of experimental results

Our results coupled with nanoindentation and HR-TEM experiments can be used to estimate the degree of crosslinking in soot particles. A diesel soot particle tested by nanoindentation (particle D1B in Ref. [23]) has been chosen for the analysis. For this experiment, the hardness value and the load-displacement of the particle were reported [23]. The particle has a hardness value of 2.5 GPa, maximum load of 3 μN and a maximum slope of the unloading stage curve of 0.85 μN/nm. From this information, it has been possible to calculate the particle contact area ($A_c = 1120$ nm^2) and Young's modulus ($E = 21$ GPa) using Eq. 2 and Eq. 4, respectively. A Poisson's ratio of 0.2 (see Appendix A.4) has been used to calculate the Young's modulus. This value correspond to $CL \approx 3$ and it is then reasonable looking at the corresponding range found for particle D1B in Section 4 ($CL_{\text{core}} = 1.5 - 3$ and $CL_{\text{shell}} = 2.6 - 3.4$) and being the mechanical properties mainly dependent to the surface properties.

A simulated TEM image of a particle with degree of crosslinking in the core and shell in the range found for particle D1B has been also reported in Fig. 11. The high resolution transmission electron microscopy image was simulated using the multislice electron microscopy software CompuTEM by Kirkland [27]. Parameters used for the simulation were: beam energy 200 kV; objective aperture 20 mrad; (-C10)df 10 nm; ddf 20 nm; with sampling image size of 1024×1024 pixels; slice thickness 0.2 nm. These parameters provide phase contrast imaging of the fringes as dark fringes.

References

[1] B. D. Adamson, S. A. Skeen, M. Ahmed, and N. Hansen. Detection of aliphatically bridged multi-core polycyclic aromatic hydrocarbons in sooting flames with atmospheric-sampling high-resolution tandem mass spectrometry. *Journal of Physical Chemistry A*, 122(48):9338–9349, 2018. doi:10.1021/acs.jpca.8b08947.

[2] B. Apicella, P. Pré, M. Alfè, A. Ciajolo, V. Gargiulo, C. Russo, A. Tregrossi, D. Deldique, and J. N. Rouzaud. Soot nanostructure evolution in premixed flames by high resolution electron transmission microscopy (HR-TEM). *Proceedings of the Combustion Institute*, 35(2):1895–1902, 2015. doi:10.1016/j.proci.2014.06.121.

[3] H. Bhowmick and S. K. Biswas. Relationship between physical structure and tribology of single soot particles generated by burning ethylene. *Tribology Letters*, 44(2): 139–149, 2011. doi:10.1007/s11249-011-9831-5.

[4] H. Bhowmick, S. K. Majumdar, and S. K. Biswas. Dry tribology and nanomechanics of gaseous flame soot in comparison with carbon black and diesel soot. *Proceedings of the Institution of Mechanical Engineers, Part C: Journal of Mechanical Engineering Science*, 226(2):394–402, 2011. doi:10.1177/0954406211429410.

[5] T. C. Bond, S. J. Doherty, D. W. Fahey, P. M. Forster, T. Berntsen, B. J. Deangelo, and et al. Bounding the role of black carbon in the climate system: A scientific assessment. *Journal of Geophysical Research Atmospheres*, 118(11):5380–5552, 2013. doi:10.1002/jgrd.50171.

[6] M. L. Botero, E. M. Adkins, S. González-Calera, H. Miller, and M. Kraft. PAH structure analysis of soot in a non-premixed flame using high-resolution transmission electron microscopy and optical band gap analysis. *Combustion and Flame*, 164:250–258, 2016. doi:10.1016/j.combustflame.2015.11.022.

[7] M. L. Botero, D. Chen, S. González-Calera, D. Jefferson, and M. Kraft. HR-TEM evaluation of soot particles produced by the non-premixed combustion of liquid fuels. *Carbon*, 96:459–473, 2016. doi:10.1016/j.carbon.2015.09.077.

[8] M. L. Botero, N. Eaves, J. A. Dreyer, Y. Sheng, J. Akroyd, W. Yang, and M. Kraft. Experimental and numerical study of the evolution of soot primary particles in a diffusion flame. *Proceedings of the Combustion Institute*, 37:2047–2055, 2019. doi:doi.org/10.1016/j.proci.2018.06.185.

[9] M. L. Botero, Y. Sheng, J. Akroyd, J. W. Martin, J. A. H. Dreyer, W. Yang, and M. Kraft. Internal structure of soot particles in a diffusion flame. *Carbon*, 141: 635–642, 2019. doi:10.1016/j.carbon.2018.09.063.

[10] K. Bowal, J. W. Martin, and M. Kraft. Partitioning of polycyclic aromatic hydrocarbons in heterogeneous clusters. *Carbon*, 143:247–256, 2019. doi:10.1016/j.carbon.2018.11.004.

[11] M. Commodo, G. De Falco, A. Bruno, C. Borriello, P. Minutolo, and A. D'Anna. Physicochemical evolution of nascent soot particles in a laminar premixed flame: from nucleation to early growth. *Combustion and Flame*, 162(10):3854–3863, 2015. doi:10.1016/j.combustflame.2015.07.022.

[12] M. Commodo, G. De Falco, P. Minutolo, and A. D'Anna. Structure and size of soot nanoparticles in laminar premixed flames at different equivalence ratios. *Fuel*, 216: 456–462, 2018. doi:10.1016/j.fuel.2017.12.032.

[13] M. Commodo, K. Kaiser, G. De Falco, P. Minutolo, F. Schulz, A. D'Anna, and L. Gross. On the early stages of soot formation: Molecular structure elucidation by high-resolution atomic force microscopy. *Combustion and Flame*, 205:154–164, 2019. doi:10.1016/j.combustflame.2019.03.042.

[14] A. D'Anna, A. Violi, A. D'Alessio, and A. F. Sarofim. A reaction pathway for nanoparticle formation in rich premixed flames. *Combustion and Flame*, 127(1-2): 1995–2003, 2001. doi:10.1016/S0010-2180(01)00303-0.

[15] S. di Stasio. Electron microscopy evidence of aggregation under three different size scales for soot nanoparticles in flame. *Carbon*, 39(1):109–118, 2001. doi:10.1016/S0008-6223(00)00099-3.

[16] R. A. Dobbins and C. M. Megaridis. Morphology of flame-generated soot as determined by thermophoretic sampling. *Langmuir*, 3(2):254–259, 1987. doi:10.1021/la00074a019.

[17] C. G. Fernández, S. Picaud, and M. Devel. Calculations of the mass absorption cross sections for carbonaceous nanoparticles modeling soot. *Journal of Quantitative Spectroscopy and Radiative Transfer*, 164:69 – 81, 2015. doi:10.1016/j.jqsrt.2015.05.011.

[18] V. Fernandez-Alos, J. K. Watson, R. vander Wal, and J. P. Mathews. Soot and char molecular representations generated directly from HR-TEM lattice fringe images using Fringe3D. *Combustion and Flame*, 158(9):1807–1813, 2011. doi:10.1016/j.combustflame.2011.01.003.

[19] G. Hantal, S. Picaud, P. N. Hoang, V. P. Voloshin, N. N. Medvedev, and P. Jedlovszky. Water adsorption isotherms on porous onionlike carbonaceous particles. Simulations with the grand canonical Monte Carlo method. *The Journal of Chemical Physics*, 133(14):144702, 2010. doi:10.1063/1.3496466.

[20] K. Hayashida, S. Nagaoka, and H. Ishitani. Growth and oxidation of graphitic crystallites in soot particles within a laminar diffusion flame. *Fuel*, 128(6):148–154, 2014. doi:10.1016/j.fuel.2014.03.008.

[21] S. Iavarone, L. Pascazio, M. Sirignano, A. De Candia, A. Fierro, L. de Arcangelis, and A. D'Anna. Molecular dynamics simulations of incipient carbonaceous nanoparticle formation at flame conditions. *Combustion Theory and Modelling*, 21 (1):49–61, 2017. doi:10.1080/13647830.2016.1242156.

[22] T. Ishiguro, Y. Takatori, and K. Akihama. Microstructure of diesel soot particles probed by electron microscopy: First observation of inner core and outer shell. *Combustion and Flame*, 108(1):231–234, 1997. doi:10.1016/S0010-2180(96)00206-4.

[23] I. Z. Jenei, F. Dassenoy, T. Epicier, A. Khajeh, A. Martini, D. Uy, and et al. Mechanical characterization of diesel soot nanoparticles: in situ compression in a transmission electron microscope and simulations. *Nanotechnology*, 29:085703, 2018. doi:10.1088/1361-6528/aaa2aa.

[24] I. Z. Jenei, F. Dassenoy, T. Epicier, A. Khajeh, A. Martini, D. Uy, H. Ghaedni, and A. Gangopadhyay. Mechanical response of gasoline soot nanoparticles under compression: An in situ TEM study. *Tribology International*, 131:446–453, 2019. doi:10.1016/j.triboint.2018.11.001.

[25] K. O. Johansson, T. Dillstrom, P. Elvati, M. F. Campbell, P. E. Schrader, D. M. Popolan-vaida, N. Richards-Henderson, K. Wilson, A. Violi, and H. A. Michelsen. Radical-radical reactions, pyrene nucleation, and incipient soot formation in combustion. *Proceedings of the Combustion Institute*, 36(1):799–806, 2017. doi:10.1016/j.proci.2016.07.130.

[26] K. O. Johansson, M. P. Head-Gordon, P. E. Schrader, K. R. Wilson, and H. A. Michelsen. Resonance-stabilized hydrocarbon-radical chain reactions may explain soot inception and growth. *Science*, 361:997–1000, 2018. doi:10.1126/science.aat3417.

[27] E. J. Kirkland. *Advanced computing in electron microscopy*. Springer Science & Business Media, 2010.

[28] P. J. Landrigan, R. Fuller, N. J. R. Acosta, O. Adeyi, R. Arnold, N. N. Basu, and et al. The Lancet Commission on pollution and health. *The Lancet.* , 2017. doi:10.1016/S0140-6736(17)32345-0.

[29] C. Lee, X. Wei, J. Kysar, and J. Hone. Measurement of the elastic properties and intrinsic strength of monolayer graphene. *Science*, 321:385–388, 2008. doi:10.1126/science.1157996.

[30] Q. Mao, A. C. T. van Duin, and K. H. Luo. Formation of incipient soot particles from polycyclic aromatic hydrocarbons: A ReaxFF molecular dynamics study. *Carbon*, 121:380–388, 2017. doi:10.1016/j.carbon.2017.06.009.

[31] Q. Mao, D. Hou, K. H. Luo, and X. You. Dimerization of polycyclic aromatic hydrocarbon molecules and radicals under flame conditions. *Journal of Physical Chemistry A*, 122:8701–8708, 2018. doi:10.1021/acs.jpca.8b07102.

[32] L. Martinez, R. Andrade, E. G. Birgin, and J. M. Martínez. PACKMOL: A package for building initial configurations for molecular dynamics simulations. *Journal of Computational Chemistry*, 30(13):2157–2164, 2009. doi:10.1002/jcc.21224.

[33] A. Oberlin. Carbonization and graphitization. *Carbon*, 22(6):521–541, 1984. doi:10.1016/0008-6223(84)90086-1.

[34] T. C. O'Connor, J. Andzelm, and M. O. Robbins. AIREBO-M: A reactive model for hydrocarbons at extreme pressures. *The Journal of Chemical Physics*, 142(2): 024903, 2015. doi:10.1063/1.4905549.

[35] W. C. Oliver and G. M. Pharr. Measurement of hardness and elastic modulus by instrumented indentation: Advances in understanding and refinements to methodology. *J. Mater. Res.*, 19(1):3–20, 2004. doi:10.1557/jmr.2004.19.1.3.

[36] L. Pascazio, M. Sirignano, and A. D'Anna. Simulating the morphology of clusters of polycyclic aromatic hydrocarbons: The influence of the intermolecular potential. *Combustion and Flame*, 185:53–62, 2017. doi:10.1016/j.combustflame.2017.07.003.

[37] L. Pascazio, J. W. Martin, M. L. Botero, M. Sirignano, A. D'Anna, and M. Kraft. Mechanical properties of soot particles: the impact of crosslinked polycyclic aromatic hydrocarbons. *Combustion Science and Technology*, 2019. doi:10.1080/00102202.2019.1668380.

[38] J. R. Patterson, S. A. Catledge, Y. K. Vohra, J. Akella, and S. T. Weir. Electrical and mechanical properties of C_{70} fullerene and graphite under high pressures studied using designer diamond anvils. *Physical Review Letters*, 85(25):5364–5367, 2000. doi:10.1103/PhysRevLett.85.5364.

[39] S. Plimpton. Fast parallel algorithms for short-range molecular dynamics. *Journal of Computational Physics*, 117(1):1–19, 1995. doi:10.1006/jcph.1995.1039.

[40] M. Rapacioli, F. Calvo, F. Spiegelman, C. Joblin, and D. J. Wales. Stacked clusters of polycyclic aromatic hydrocarbon molecules. *The Journal of Physical Chemistry A*, 109(11):2487–2497, 2005. doi:10.1021/jp046745z.

[41] K. Rego and V. Meunier. Carbon nanotube knots. *AIP Advances*, 9:025030, 2019. doi:10.1063/1.5088145.

[42] H. Richter, T. G. Benish, O. A. Mazyar, W. H. Green, and J. B. Howard. Formation of polycyclic aromatic hydrocarbons and their radicals in a nearly sooting premixed benzene flame. *Proceedings of the Combustion Institute*, 28(2):2609–2618, 2000. doi:10.1016/S0082-0784(00)80679-7.

[43] F. Schulz, M. Commodo, K. Kaiser, G. De Falco, P. Minutolo, G. Meyer, A. D'Anna, and L. Gross. Insights into incipient soot formation by atomic force microscopy. *Proceedings of the Combustion Institute*, 37(1):885–892, 2019. doi:10.1016/j.proci.2018.06.100.

[44] R. H. Shim, H. S.and Hurt and N. Yang. A methodology for analysis of 002 lattice fringe images and its application to combustion-derived carbons. *Carbon*, 38(1): 29–45, 2000. doi:10.1016/S0008-6223(99)00096-2.

[45] M. S. Solum, A. F. Sarofim, R. J. Pugmire, T. H. Fletcher, and H. Zhang. ^{13}C NMR analysis of soot produced from model compounds and a coal. 15:961–971, 2001. doi:10.1021/ef0100294?rand=qp6ntlo5.

[46] S. J. Stuart, A. B. Tutein, and J. A. Harrison. A reactive potential for hydrocarbons with intermolecular interactions. *The Journal of Chemical Physics*, 112(14):6472–6486, 2000. doi:10.1063/1.481208.

[47] T. S. Totton, A. J. Misquitta, and M. Kraft. A quantitative study of the clustering of polycyclic aromatic hydrocarbons at high temperatures. *Physical Chemistry Chemical Physics*, 14(12):4081–4094, 2012. doi:10.1039/c2cp23008a.

[48] R. S. Tranter, S. J. Klippenstein, L. B. Harding, B. R. Giri, X. Yang, and J. H. Kiefer. Experimental and theoretical investigation of the self-reaction of phenyl radicals. *The Journal of Physical Chemistry A*, 114(32):8240–8261, 2010. doi:10.1021/jp1031064.

[49] R. Vander Wal. A TEM methodology for the study of soot particle structure. *Combustion Science and Technology*, 126(1-6):333–351, 1997. doi:10.1080/00102209708935680.

[50] A. Violi, A. Kubota, T. Truong, W. Pitz, C. Westbrook, and A. Sarofim. A fully integrated kinetic Monte Carlo/molecular dynamics approach for the simulation of soot precursor growth. *Proceedings of the Combustion Institute*, 29(2):2343–2349, 2002. doi:10.1016/S1540-7489(02)80285-1.

[51] A. Violi, A. F. Sarofim, and G. A. Voth. Kinetic Monte Carlo-molecular dynamics approach to model soot inception. *Combustion Science and Technology*, 176(5-6): 991–1005, 2004. doi:10.1080/00102200490428594.

[52] C. Wang, T. Huddle, C. H. Huang, W. Zhu, R. L. Vander Wal, E. H. Lester, and J. P. Mathews. Improved quantification of curvature in high-resolution transmission electron microscopy lattice fringe micrographs of soots. *Carbon*, 117:174–181, 2017. doi:10.1016/j.carbon.2017.02.059.

[53] H. Wang. Formation of nascent soot and other condensed-phase materials in flames. *Proceedings of the Combustion Institute*, 33(1):41–67, 2011. doi:10.1016/j.proci.2010.09.009.

[54] K. Yehliu, R. L. Vander Wal, and A. L. Boehman. Development of an HR-TEM image analysis method to quantify carbon nanostructure. *Combustion and Flame*, 158(9):1837–1851, 2011. doi:10.1016/j.combustflame.2011.01.009.

[55] B. Zhao, K. Uchikawa, and H. Wang. A comparative study of nanoparticles in premixed flames by scanning mobility particle sizer, small angle neutron scattering, and transmission electron microscopy. *Proceedings of the Combustion Institute*, 31: 851–860, 2007. doi:10.1016/j.proci.2006.08.064.

[56] H. Zhao, K. Min, and N. R. Aluru. Size and Chirality Dependent Elastic Properties of Graphene Nanoribbons under Uniaxial Tension. *Nano Letters*, 9(8):3012–3015, 2009. doi:10.1021/nl901448z.

[57] G. A. Zickler, T. Schöberl, and O. Paris. Mechanical properties of pyrolysed wood: a nanoindentation study. *Philosophical Magazine*, 86(10):1373–1386, 2006. doi:10.1080/14786430500431390.